JMEPEG (2009) 18:1144–1150
DOI: 10.1007/s11665-009-9355-4

1059-9495/$19.00

Texture Distribution and Plane Strain Mechanical Behavior of AA 7xxx Plates of Different Thicknesses

Gonzalo Becerra, Jorge Ramos-Grez, and José Montecinos

(Submitted September 12, 2006; in revised form December 17, 2008)

Texture distribution of a rolled aluminum alloy type AA 7449 plate having two thicknesses is presented here. The mechanical behavior of these aluminum alloy plates under plane strain compression (PSC) was studied under different shear stress textures. Crystallographic texture of specimens was characterized by x-ray diffraction and the corresponding volume fractions of each texture component were determined. The obtained results show that shear stress texture components are concentrated at layers immediately below the surface, as it had been previously proposed. Additionally, specimens were subjected to hot PSC to mimic industrial hot rolling process under controlled conditions. The measured rheological parameters, strain rate sensitivity coefficient *m*, and activation energy *Q*, show that the mechanical behavior under PSC is more sensitive to test conditions than to the shear stress texture.

Keywords advanced characterization, aluminum, mechanical testing, rolling

1. Introduction

The 7xxx series aluminum alloys have been developed over the last 50 years in response to the demands imposed by the aircraft industry (Ref 1). Structural components found in wings and ailerons are currently fabricated out of these alloys. According to Morere (Ref 2), this type of alloys are required to have high ductility and high rupture strength together with low-cycle fatigue resistance and high stress corrosion strength. On this context, the manufacture of metal products out of these alloys generally includes one or more stages of hot forming, such as rolling, extrusion, or forging. These processing steps provide finished products and also semi-finished products which then will be cold formed. Chovet-Sauvage (Ref 3) indicates that the final mechanical properties of this type of alloys would strongly depend on microstructure and texture developed during forming. For example, Salamci (Ref 4) studied the behavior of Al-7075 alloy after extrusion indicating that $<111>$ and $<100>$ fiber textures lead to higher mechanical properties in the longitudinal direction. Complementary, Wang et al. (Ref 5) used (electron back-scatter diffraction) EBSD to analyze crystallographic texture on Al-7034 alloy after processing through equal-channel angular pressing (ECAP). They found that after one pass processing, the $<111>$ fiber texture is relative stable while the $<001>$ evolves to a $\{001\}<100>$ texture.

Gonzalo Becerra, Jorge Ramos-Grez, and **José Montecinos**, Departamento de Ingeniería Mecánica y Metalúrgica, Escuela de Ingeniería, Pontificia Universidad Católica de Chile, Vicuña Mackenna 4860, Código Postal 6904411 Santiago, Chile. Contact e-mail: jramos@ing.puc.cl.

On the other hand, hot rolling is a well-established deformation process commonly used in the metal-forming industry (Ref 6). It is known that hot rolling produces a state of plane strain compression (PSC), or equivalently a bi-dimensional deformation state on the material. According to Driver and Engler (Ref 7), the latter deformation state is specifically located at the central layers; whereas at the surface, due to the contact between the material and the rolls, it produces a combined PSC and shear state. A shear component can then affect texture and microstructure, and thus the mechanical properties at the surface of the rolled material. Several authors have proposed two main reasons for this texture inhomogeneity which is developed along the thickness of a rolled sheet. Asbeck and Mecking (Ref 8) attributed this inhomogeneity to the friction that exits between the rolls and the material and that its effect is restricted to a thin surface layer of the order of the rolls roughness (0.01-0.05 mm). The second reason according to Truszkowski et al. (Ref 9) is the nonuniformity in penetration of the shear deformation through the thickness of the material. This latter effect is related to the parameter l/h (l: length of the contact surface between rolls and material, h: final thickness of the material). Moreover, it is considered that this shearing effect is basically the origin of texture inhomogeneities on hot-rolled metals. Asbeck and Mecking (Ref 8) concluded that inhomogeneities in texture are developed across the sample thickness when the ratio l/h is smaller than 0.5. On other hand, the same authors stated that when $l/h > 0.5$ textures become homogeneous. However, Truszkowski et al. (Ref 9) concluded that rolling with large values of the l/h ratio leads to the formation of a shear texture at the surface of the sheet which then penetrates toward the intermediate layer. Whereas for values of $l/h \sim 0.5$, the shear texture appears only at the intermediate layer.

The present research work examines texture development and mechanical properties along the thickness of two hot-rolled 7xxx aluminum alloy plates, 40 mm and 24 mm thick, provided by ALCAN Research Center Voreppe (CRV). The first part of the study focuses on the influence of the plate thickness on texture distribution after hot rolling. This includes

the determination of the layers inside the plate with the most significant texture difference. In all situations, texture was characterized by x-ray diffraction. During the second part of the study, the influence of shear texture on the mechanical properties of the rolled aluminum alloy plate was studied. For this purpose, hot plane deformation tests were performed on specimens taken out from the previously 40-mm-thick rolled aluminum plate at different layers along its depth. Their rheological parameters were then measured and analysed. Hot-rolling conditions were simulated by instrumented high-temperature plane strain channel-die compression tests under constant temperature and strain rate. The standard rheological parameters

$$m = \left.\frac{\partial \ln \sigma}{\partial \ln \dot{\varepsilon}}\right|_T \quad \text{(Eq 1)}$$

and the activation energy for deformation

$$Q = \left.\frac{R}{m}\frac{\partial \ln \sigma}{\partial (1/T)}\right|_{\dot{\varepsilon}} \quad \text{(Eq 2)}$$

were obtained out of the measured results. From the latter, the Zener-Hollomon parameter was computed as

$$Z = \dot{\varepsilon} \exp\left(\frac{Q}{RT}\right) \quad \text{(Eq 3)}$$

Finally, the flow stress was estimated by a power law of the form

$$\sigma_s = A * Z^m \quad \text{(Eq 4)}$$

as suggested by Driver and Engler (Ref 7).

2. Experimental Procedure

The alloy had a composition close to that of the AA 7449 alloy (7.5-8.7% Zn, 1.8-2.7% Mg, 1.4-2.1% Cu, and 0.25% Zr + Ti) and was supplied by Alcan CRV. The Zr content ensures that none or little recrystallization occurs during or after hot rolling so that texture variations are purely strain dependent. The as-received materials had been hot rolled under industrial conditions in a reversible mill to final thicknesses of 40 mm and 24 mm, respectively. The convention used for the geometry of flat rolling is adopted, with ND being the compression direction, RD the extension direction, and TD the direction constrained by the channel. Five specimens of dimensions 5 mm × 30 mm × 26 mm were cut in the (RD, TD) plane, from the centre of the test coupon ($L = 0$) up to the surface of it ($L = 1$), for each material. After that, texture measurements were performed by x-ray diffraction technique using the $<111>$ pole figures. On the other hand, volume fractions of the texture components were calculated using an improved version of the software developed by Van Houtt (Ref 10).

Based on the results obtained, two groups of rectangular specimens of dimension (15 mm × 10 mm × 7 mm and 10 mm × 8 mm × 7 mm) were additionally taken out from the 40 mm thick material from layers (i.e., $L = 0$ and $L = 0.75$) having the highest difference in shear texture, respectively. These were then deformed under hot PSC to a logarithmic strain of 1 at temperatures of 250 and 500 °C. Table 1 shows the test conditions for each specimen, as well as their real dimensions. Plane strain channel-die compression tests were conducted using a mechanical device described elsewhere by Maurice and Driver (Ref 11) and Morere et al. (Ref 12), which was attached to a Schenck servo-hydraulic machine to compress the specimens at constant strain rates of 1 and 10 s^{-1}. This device is located at the École Nationale Supérieure des Mines de Saint-Etienne (EMSE, France). This equipment enables the specimen to be water quenched within 2 s from the end of deformation process. To reduce friction effects, the specimens were first coated with graphite (Acheson liquid) and then wrapped up in Teflon films (0.05 mm thick). Comparative hot uniaxial and PSC tests previously done by Karhausen et al. (Ref 13) and Maurice et al. (Ref 14) on aluminum polycrystalline alloys have conclusively demonstrated that the latter method gives very good flow stress reproducibility and low friction coefficients estimated at 0.01-0.02. Texture measurements were again performed by x-ray diffraction technique on each specimen and the volume fractions of the texture components were calculated as indicated before.

Table 1 Specimens real dimensions and hot deformation testing conditions

Specimen no.	Temperature-Strain rate-strain	l_0, mm	t_0, mm	t_f, mm	$\bar{\varepsilon}$	$\dot{\bar{\varepsilon}}$, s^{-1}
1	250 °C-1 s^{-1}-1	7.97	10.02	4.44	0.94	0.959
2	250 °C-1 s^{-1}-1	7.99	10.02	4.45	0.94	0.955
3	250 °C-1 s^{-1}-1	10.00	15.00	6.40	0.98	0.952
4	500 °C-1 s^{-1}-1	8.00	10.03	4.02	1.06	0.968
5	500 °C-1 s^{-1}-1	7.98	10.03	3.93	1.08	0.963
6	500 °C-1 s^{-1}-1	10.00	15.00	6.23	1.01	1.008
7	500 °C-10 s^{-1}-1	8.00	10.01	4.31	0.97	9.587
8	500 °C-10 s^{-1}-1	7.98	10.01	4.34	0.97	9.634
9	500 °C-10 s^{-1}-1	9.99	14.98	6.23	1.01	10.2

3. Results

The experimental results are divided into two sections: one presenting the texture results obtained from the as-received material while the second section shows the hot deformation results.

3.1 Texture Results Obtained from the As-Received Material

Concerning the texture results obtained from the as-received material, Fig. 1 shows the texture maps obtained from five layers in each material. For the 40-mm-thick material (Table 2), it is seen that the central layers ($L = 0$ to $L = 0.5$) present a classical hot-rolling texture (PSC), where the β-fiber can be seen on the $<111>$ pole figure; the volume fractions show that the β-fiber components values (sum of Brass, S and Copper components) are high and almost constant (∼65%). The $L = 0.75$ layer has a different texture, with a highly disordered orientation, where no PSC texture can be seen. The volume fractions show that the shear stress produced by the rolls decreased the β-fiber components (∼12%) and the shear texture component (CT45 ND) is ∼12%. At the surface layer ($L = 1$), the texture acquires the common hot-rolling texture, although the β-fiber is lower than the central layers (∼53%) and the value of CT45 ND is ∼3%. The latter observation suggests the negligible influence the shear stresses have on the surface texture.

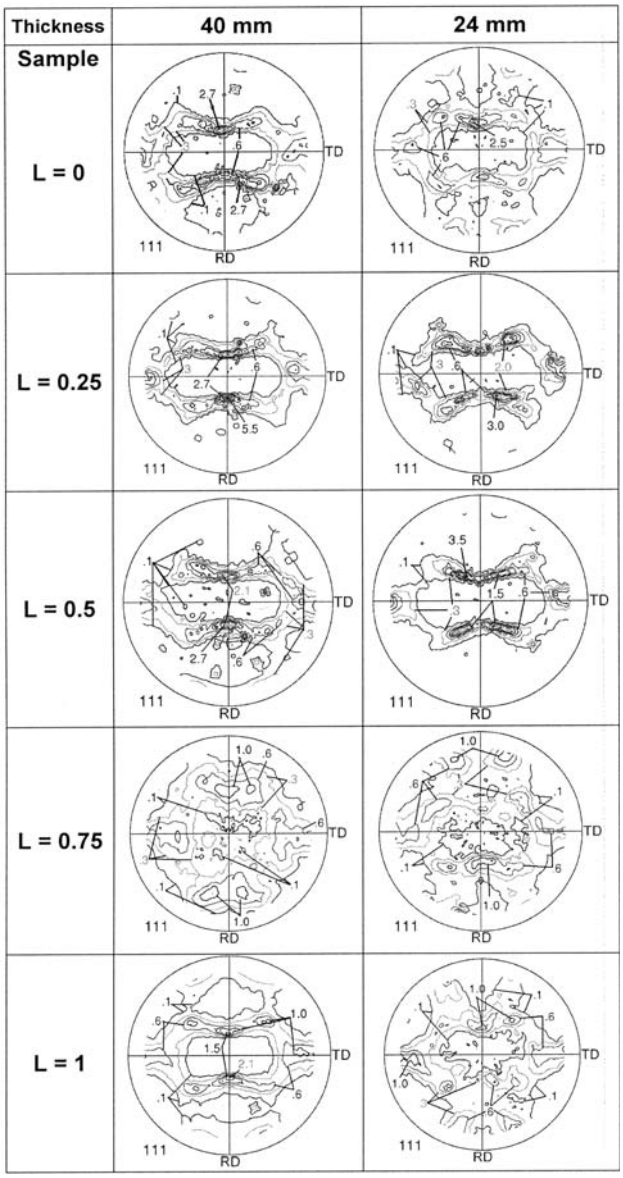

Fig. 1 (111) Pole figures for the materials samples

Table 2 Volume fraction of the principal components (%) of the 40-mm-thick samples

	$L = 0$	$L = 0.25$	$L = 0.5$	$L = 0.75$	$L = 1$
Cube	4.63	4.31	4.31	3.00	4.38
Copper	8.63	8.69	8.88	1.50	6.00
Brass	23.19	25.38	20.19	3.12	16.00
S	32.63	34.07	33.26	7.00	31.19
Goss	0.94	2.75	1.88	0.63	0.00
CT45 TD	0.63	0.75	0.31	0.38	0.38
CT45 ND	0.50	0.38	0.25	12.19	2.56
CT22.62	6.69	5.07	7.38	3.75	4.13
CT67.38					
Other	22.19	18.63	23.56	68.44	35.38

For the 24-mm-thick material (Table 3), it can be seen that the layers $L = 0.25$ and $L = 0.5$ exhibit a common hot-rolling texture (PSC), with a β-fiber visible on the $<111>$ pole figures.

Table 3 Volume fraction of the principal components (%) of the 24-mm-thick samples

	$L = 0$	$L = 0.25$	$L = 0.5$	$L = 0.75$	$L = 1$
Cube	4.63	9.69	2.94	7.06	5.31
Copper	3.13	4.38	4.32	2.25	3.62
Brass	13.57	25.50	37.31	8.63	8.69
S	23.12	35.12	35.82	16.07	18.95
Goss	2.13	0.50	0.44	0.75	0.06
CT45 TD	0.38	0.06	0.63	0.44	0.13
CT45 ND	4.19	0.00	0.00	3.56	4.69
CT22.62	4.69	5.82	4.87	3.5	4.87
CT67.38					
Other	44.19	18.94	13.69	57.75	53.69

The β-fiber volume fractions are 65 and 77%, respectively. On the other hand, layers $L = 0$, $L = 0.75$, and $L = 1$ have a disordered texture, where the PSC components are reduced, with β-fiber volume fractions of 40, 27, and 31%, respectively. The average CT45 ND volume fraction present in these layers is ~4.2%. The volume fractions also show that the central layer ($L = 0$) is more influenced by PSC texture and that the $L = 0.75$ layer does not have a high-shear texture presence, as also seen on the 40-mm-thick material.

3.2 Hot Deformation Results

For the second part of the study, hot deformation results obtained from specimens taken out from the 40-mm-thick material are shown in Fig. 2. These illustrate the stress-strain curves obtained for two deformation rates (1 and 10 s^{-1}) and two deformation temperatures (250 and 500 °C). The typical shape of a hot-deformation curve, characterized by the fast establishment of the maximum yield stress followed by a stationary state with some small variations thereafter, is observed at 500 °C. However, at 250 °C, a decrease in flow stress from 230 to 160 MPa has taken place. This flow softening could be due to deformation by localized shear along shear bands, as it is unlikely to have been caused by adiabatic heating of the aluminum alloy at a strain rate of 1 s^{-1}. In spite of the fact that stress-strain data were obtained for two temperatures and two deformation rates only, the calculated overall strain rate sensitivity coefficient m is 0.19 for a temperature of 500 °C, while the overall activation energy Q at this temperature corresponds to 101 kJ mol^{-1} for a strain velocity of 1 s^{-1}. Nonetheless, it was assumed that the material deformation mechanisms obey an Arrhenius type dependence with temperature.

Table 4 shows the PSC components, i.e., β-fiber (sum of Brass, S and Copper components), and shear components (CT45 ND) before and after the channel-die deformation process. It can be seen that in all specimens the PSC ratio increases almost constantly to ~71% at the layer $L = 0$ and to ~57% at layer the $L = 0.75$. On the other hand, the shear components decrease to almost zero at both layers. It can be also noticed that at the $L = 0$ layer, there is a slight increase in PSC texture (10%) and almost no variation of the shear components independently of the deformation conditions. However, at the $L = 0.75$ layer, a 5.2-fold increase of PSC components and a 32-fold decrease of shear components have taken place. Finally, Table 5 indicates the percentage volume fractions of the principal components of the channel-die tested specimens.

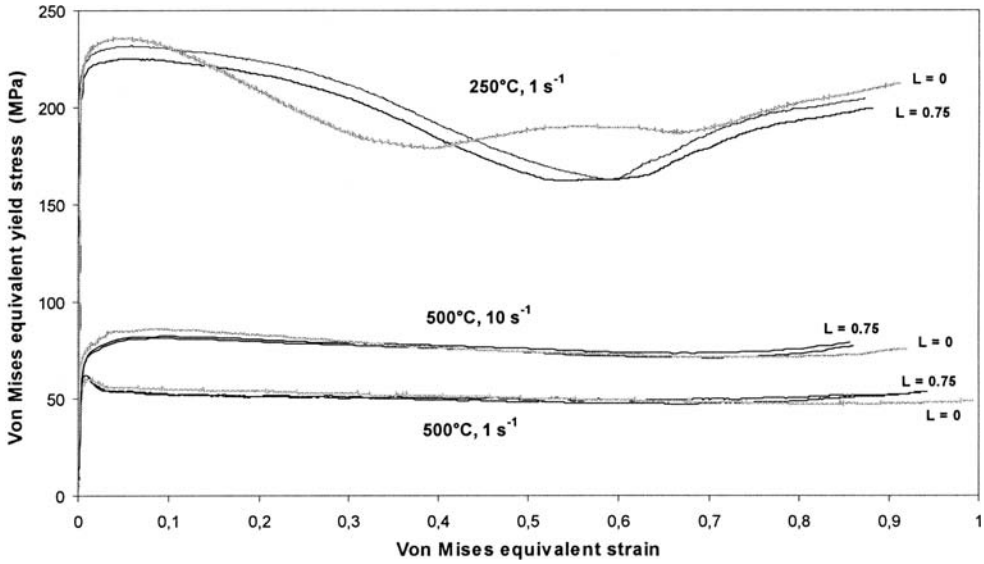

Fig. 2 Stress vs. deformation curves of Channel-die plane strain compression tests

Table 4 PSC and shear components evolution, for all deformed conditions and layers, before and after the channel-die test

	250 °C, 1 s^{-1}		500 °C, 1 s^{-1}		500 °C, 10 s^{-1}	
	$L = 0$	$L = 0.75$	$L = 0$	$L = 0.75$	$L = 0$	$L = 0.75$
Before channel-die						
PSC (β fiber)	64.45	11.62	64.45	11.62	64.45	11.62
Shear (CT45 ND)	0.50	12.19	0.50	12.19	0.50	12.19
After channel-die						
PSC (β fiber)	71.94	60.50	70.08	54.63	71.56	58.20
Shear (CT45 ND)	0.00	0.38	0.31	0.38	0.25	0.13

Table 5 Volume fraction of the principal components (%) found on the channel-die tested samples

	250 °C, 1 s^{-1}		500 °C, 1 s^{-1}		500 °C, 10 s^{-1}	
	$L = 0$	$L = 0.75$	$L = 0$	$L = 0.75$	$L = 0$	$L = 0.75$
Cube	2.63	4.25	5.94	9.63	6.81	9.19
Copper	9.25	9.25	5.00	6.19	3.63	6.19
Brass	29.81	17.75	34.26	18.57	31.50	20.94
S	32.88	33.50	30.82	29.87	36.76	31.07
Goss	1.06	1.50	1.13	1.06	0.88	1.19
CT45 TD	0.06	0.06	0.75	0.06	1.13	0.44
CT45 ND	0.00	0.38	0.31	0.38	0.25	0.13
CT22,62 CT67,38	3.12	4.94	6.44	6.32	8.12	6.00
Others	21.19	28.56	15.38	27.94	10.94	24.88

4. Discussion of Results

The discussion of the obtained experimental results is also divided into two sections, one based on the influence of specimen thickness on shear texture distribution while the second one provides insight about the influence of shear texture content on hot strain mechanical behavior for a given hot-rolled plate thickness.

4.1 Influence of Specimen Thickness on Texture Distribution

To provide a better visualization of the measured texture distribution, plots of the experimental results obtained from the studied 7xxx series alloy material are presented on Fig. 3. On these graphs, the texture components related to shear strain appears at a location of $L = 0.75$ for the 40 mm material; and at the $L = 0$ (low intensity) and $L > 0.7$ for the 24 mm material. The graph's input data correspond to the addition of the principal shear strain components that are shown on the volumes fraction tables (i.e., CT45 ND and CT45 TD). A sixth degree polynomial was fitted to each set of points to represent the texture distribution with the best possible fit. The mean squared error obtained for each set of plotted points was equal to 0.66 and 1.32 for 40-mm and 24-mm thick materials, respectively. These shear texture distributions allow comparison with other distributions published somewhere else, such as those obtained by Truszkowski et al. (Ref 9). However, the presented fitted curves show a different distribution when compared to the curves obtained by the latter author, which describe a shear texture distribution with a constant penetration from the surface to the centre. Moreover, from Fig. 3, it can be observed that the distribution of shear texture is influenced by the final thickness of the material after rolling. As the thickness of the plate increases, it produces a decrease on the quantity of shear stress components and a more uniform distribution of the PSC components, especially at the central zone of the specimen. In fact, it can be seen that maximum values of the fitted polynomial curves do not take place on the superficial layer, but in the layer immediately below it (i.e., $L \sim 0.8$ for 40 mm and $L \sim 0.9$ for 24 mm). This is could be explained by the surface layer displacement due to the rolls roughness, the impingement over the surface and a shear distribution that penetrates the material from the surface to the centre as described by Truszkowski et al. (Ref 9).

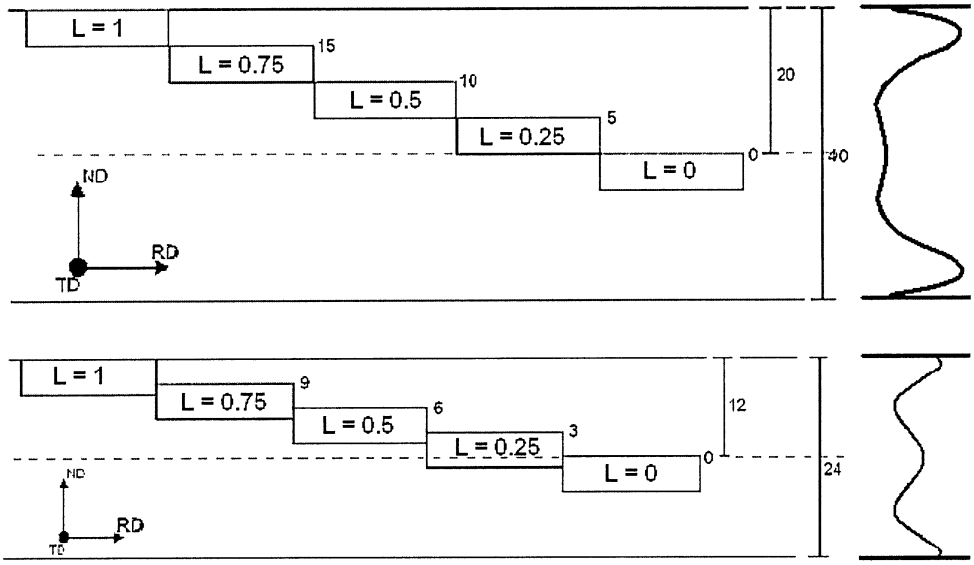

Fig. 3 Texture intensities diagrams corresponding to the 40-mm and 24-mm-thick plates

A mechanism for the formation of shear texture can be found in Tselikov's model of deformation of metals in the rolling gap (Ref 15). This model predicts different scenarios corresponding to rolling process carried out on sheets rolled at different values of the l/h ratio: (a) $l/h > 5$; (b) $l/h = 2\text{-}5$; (c) $l/h = 0.5\text{-}2$; and (d) $l/h < 0.5$. In each case, the normal stress changes as well as the value of the unit friction force at the sheet surface. Tselikov's model, which considers friction on the surface of the rolled sheet, predicts shear strain only for high values of the l/h ratio. Hence, in our situation, the maxima are located as much on the superficial layers as on the intermediate; this can be attributed to the interaction of different effects such as friction behind and in front of the neutral plane. Additionally, it must be considered that the neutral plane itself changes its position with decreasing l/h ratio. Formation of a shear texture at intermediate layers when l/h ratio is small may not be necessarily explained by Tselikov's model. The latter only considers the direct influence of the friction force on the surface of the sheet.

4.2 Influence of Shear Texture on the Hot Strain Mechanical Behavior

The following analysis is based on the results obtained from the specimens subjected to hot PSC that were in turn extracted from two selected layers taken out of the 40-mm-thick plate with most significantly texture difference, $L = 0$ (high PSC) and $L = 0.75$ (high-shear texture). For the determination of quantitative differences, the rheological parameters of the hot plane compression tests were calculated. It must be emphasized that the stress-strain data were measured at two specific temperatures and strain rates. The obtained results are the following.

4.2.1 Stress-Strain Curves. All the deformation curves presented on Fig. 2 show a very similar response, with no significant differences of their mechanical strength, since percentage differences at the maximum peak of yield stress do not exceed 7% in all cases.

4.2.2 Strain Rate Sensitivity Coefficient. Variations of flow stress σ (measured at a real strain of $\varepsilon = 0.2$) as function of strain rate are showed in Fig. 4 for a given deformation temperature and for each selected layer ($L = 0$ and $L = 0.75$). The calculated coefficient values are $m_0 = 0.1874$ and $m_{0.75} = 0.1932$, both for a test temperature of 500 °C. These values were calculated using Eq 1 and are very close to the overall value ($m = 0.1913$), respectively. Over the strain rate interval considered (1-10 s^{-1}), the strain rate sensitivity coefficient is constant for the given deformation temperature.

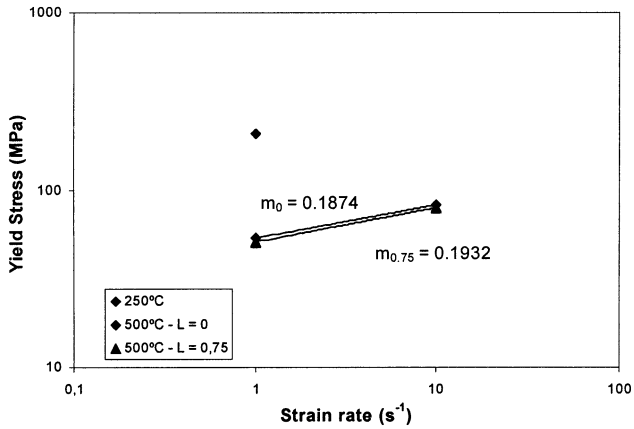

Fig. 4 Evolution of flow stress at a strain of 0.2 as a function of strain rate. The curve's slope gives the strain rate sensitivity coefficient (m) for both layers

4.2.3 Activation Energy. The apparent activation energy Q, which indicates the sensitivity of yield stress to temperature, was calculated using Eq 2 from the curve presented in Fig. 5. For each value of m, an activation energy was obtained, the results were $Q_0 = 97$ kJ mol^{-1} and $Q_{0.75} = 102$ kJ mol^{-1}, for $L = 0$ and $L = 0.75$, respectively. These results show a 5% difference between them and a 4 and 1% difference, respectively, with the overall activation energy obtained ($Q = 101$ kJ mol^{-1}). It is important, however, to point out that care should be exercised on Arrhenius plots when data for only two temperatures are available, particularly when the results obtained, at one of the test temperatures, show deviations (as it happened at 250 °C).

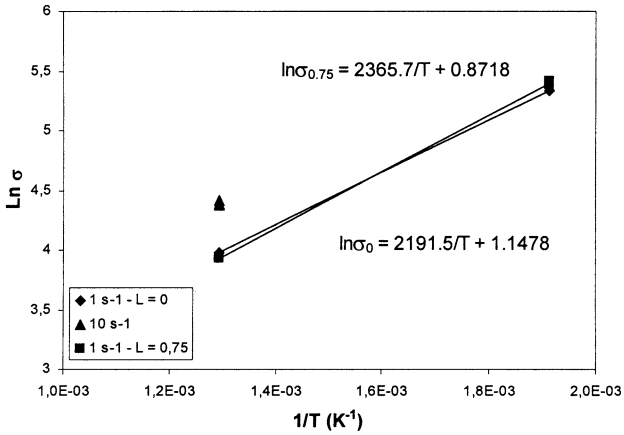

Fig. 5 Evolution of 0.2 flow stress as a function of the inverse of the test temperature. The curve's slope is equal to mQ/R, from where it can be estimated the apparent activation energy Q for each layer

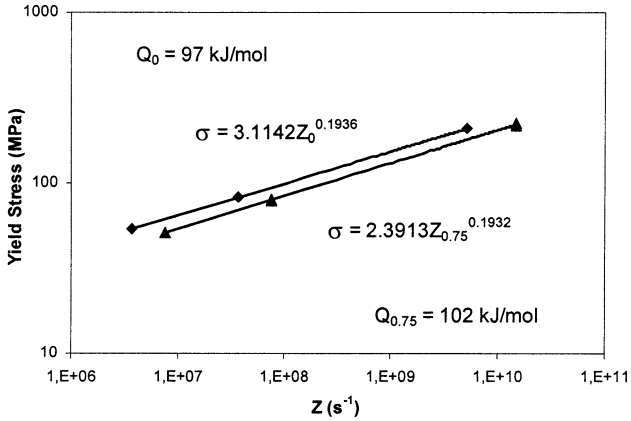

Fig. 6 Evolution of flow stress (at a strain of 0.2) as a function of the Zener-Hollomon parameter for two layers (centre $L = 0$ and quarter thickness $L = 0.75$)

4.2.4 Yield Stress Evolution as a Function of Process Conditions. Figure 6 shows the flow stress evolution as a function of the Zener-Hollomon parameter, as defined by Eq 3. This parameter is calculated using the corresponding values of the calculated activation energies. In our case, the activation energy values of 97 and 102 kJ mol^{-1} were used to obtain the values for Z_0 and $Z_{0.75}$, respectively. Representative results for each case are obtained by the relationship between flow stress and the Zener-Hollomon parameter given by Eq 4, this is $\sigma = 3.11Z_0^{0.1936}$ and $\sigma = 2.39Z_{0.75}^{0.1932}$. It can be noticed that the strain rate sensitivity values, 0.1936 and 0.1932, are near in magnitude to the overall value of m (0.1913) under the temperature interval considered. From these results, measured at $L = 0$ and $L = 0.75$, it can be inferred that the behavior of the m and Q parameters during hot deformation does not show a dependence on the shear texture indexes on the material, since their percentage difference is $<4\%$. Moreover, the Zener-Hollomon parameter verification shows that the strain rate sensitivity, obtained by this method, at different layers only differs by a 0.2%.

5. Conclusion

The principal objective of this work is to contribute to the knowledge of some of the mechanical properties that are developed during hot rolling of an AA 7449 type alloy (7xxx series). The principal conclusions that can be drawn from this research are the following:

1. The presence of a shear texture on the deformed materials does not show a constant decrease in magnitude from the surface toward the centre of the plate, as proposed by Truszkowski et al. (Ref 9). However, it has a maximum located between layers $L = 0.7$ and 0.9; being L equal to 0 at the centre and 1 at the surface. It was observed that shear texture is also present on the central layer although with less intensity.
2. The PSC presence has its maximum values at the zones between $L = 0.2$ and 0.6, approximately. As the thickness of the plate increases, PSC presence is greater and uniform through out all the material, whereas the shear texture concentrates on a thin layer with a high value. In the opposite case, the shear texture appears mainly over all the depth of the specimen, but its maximum values decrease.
3. The material's rheological parameters measured during PSC tests were not significantly dependent on the shear texture presence, since the percentage differences between the stress-strain curves were $<7\%$. This conclusion was further corroborated from the values obtained for the rheological parameters, m and Q.

Acknowledgments

This work has been carried out in fulfillment of a Master Thesis by Gonzalo Becerra co-supervised at the École Nationale Supérieure des Mines de Saint-Etienne (France) and Pontificia Universidad Católica de Chile. The authors would like to express their most sincere gratitude to the research staff at EMSE, Centre Sciences des Matériaux et des Structures, for their help during the experimental data acquisition, and to Dr. Julian Driver and Dr. David Piot for revising the early stages of this manuscript.

References

1. J. Polmear, *Light Alloys*, 3rd ed., London, Arnold, 1995
2. B. Morere, "Recristallisation d'un alliage d'aluminium 7010 après déformation à chaud; Influence sur la ténacité," Thèse de l'ENSM.SE et de l'INPG, 1999
3. C. Chovet-Sauvage, "Évolution des microstructures et des textures en grande déformation à chaud d'un alliage Al-Mg-Si," Thèse de l'ENSM.SE et de l'INPG, 2000
4. E. Salamci, Directionality in the Mechanical Properties of Spray Cast and Extruded 7xxx Series Aluminium Alloys, *Turkish J. Eng. Env. Sci.*, 2003, **27**, p 169–176
5. S.C. Wang, M.J. Starink, N. Gao, C. Xu, and T. Langdon, Grain Structure and Texture Development During ECAP of Two Heat-Tratable Al-Based Alloys, *Rev. Adv. Mater. Sci.*, 2005, **10**, p 249–255
6. J.A. Schey, *Introduction to Manufacturing Processes*, 2nd ed., McGraw Hill, New York, 1987
7. J.H. Driver and O. Engler, Design of Aluminium Rolling Processes for Foil, Sheet and Plate, Chapter 4, *Handbook of Metallurgical Process Design*, Marcel Dekker, Inc., New York, 2003, p 69–114

8. H.O. Asbeck and H. Mecking, Influence of Friction and Geometry of Deformation on Texture Inhomogeneities During Rolling of Cu Single Crystals as an Example, *Mater. Sci. Eng.*, 1978, **34**, p 111–119
9. W. Truszkowski, J. Król, and B. Major, Inhomogeneity of Rolling Texture in fcc Metals, *Metall. Trans. A*, 1980, **11A**, p 749–758
10. P. Van Houtt, *The "MTM-FHM" Software System, Version 2*, Department of Metallurgy and Materials Engineering, Katholieke Universiteit Leuven, Belgium, 2000
11. C. Maurice and J.H. Driver, High Temperature Plane Strain Compression of Cube Oriented Aluminium Crystals, *Acta Metall. Mater.*, 1993, **41**, p 1644–1653
12. B. Morere, C. Maurice, R. Shahani, and J.H. Driver, The Influence of Al 3 Zr Dispersoids on the Recrystallization of Hot-Deformed AA 7010 Alloys, *Metall. Mater. Trans. A*, 2001, **32**, p 625–632
13. K.F Karhausen, J. Savoie, C.M. Allen, D. Piot, and R. Luce, Material Testing, Constitutive Modeling and Implementation of Material Models into Hot Rolling Models for Alloy AA3103, *Mater. Sci. Forum*, 2002, **396–402**, p 371–378
14. C. Maurice, D. Piot, H. Klocker, and J.H. Driver, Hot Plane Strain Compression Testing of Aluminum Alloys by Channel-Die Compression, *Metall. Mater. Trans.*, 2005, **36A**, p 1039–1047
15. A.J. Tselikov, *Stress and Strain in Metal Rolling*, Mir Publishers, Moscow, 1961